Comparisons of VHF Meteor Radar Observations in the Middle Atmosphere With Multiple Independent Remote Sensing Techniques.

Daniel L. McIntosh, BSc. (Hons)

Thesis
submitted for the degree of
DOCTOR OF PHILOSOPHY
at the
UNIVERSITY OF ADELAIDE
School of Chemistry and Physics
Discipline of Physics

August 2009

Chapter 8

Mesospheric Temperature Comparisons

8.1 Temperatures Derived From Routine Meteor Observations

Mesospheric temperature estimates can be obtained on and about the peak height of the meteor distribution from estimates of the ambipolar diffusion coefficient. The ambipolar diffusion coefficient for a typical underdense echo is given by

$$D_a = \frac{\lambda^2}{16\pi^2\tau}, \tag{8.1}$$

where λ is the radar wavelength and τ is the measured echo decay time. The echo decay time is defined as the time it takes for the echo power $P_r(t)$ to decay to e^{-2}. A derivation of this result can be found in McKinley [1961] which assumes the radial distribution of charge to be Gaussian. Jones [1995] has shown that the distribution is more correctly described by a dense narrow core and a more diffuse central region. This however does not effect the above result. The value of the diffusion coefficient is determined by taking the natural log of the signal (see red curve in Figure 6.5) and performing a least-squares fit. The slope of the resulting fit line is then used to determine estimates of D_a [Holdsworth et al., 2004].

In order to determine atmospheric temperature T, we need to determine a relationship with the measured ambipolar diffusion coefficient. This can

be achieved through the use of the Einstein diffusion relation

$$D_i = \frac{kT_iK}{e}, \tag{8.2}$$

where D_i is the ionic diffusion coefficient for ions in a neutral gas, k is Boltzman's constant, T_i is the ionic temperature, e is the electronic charge and K is the the zero field mobility factor of the ion species in a neutral gas. K itself in fact varies with temperature; however according to Elford et al. [1998] this is $\leq 20\%$ for a change in ambient temperature of 100 K. According to Cervera and Reid [2000] K maybe scaled with respect to standard atmospheric temperature and pressure and may be written in terms of a 'reduced mobility' factor K_0 as follows

$$K = \frac{1.013 \times 10^5}{p}\frac{T}{273.16}K_0. \tag{8.3}$$

The value for K_0 depends upon the particular chemical composition of the meteor; however a value of 2.4×10^{-5} has been chosen after Cervera and Reid [2000]. Jones and Jones [1990] have shown that the value for K_0 for metallic ions depends almost exclusively upon the mass number of the of the ion. They have chosen Mg^+ and Fe^+ as having mass numbers which bracket the range of ions found in various meteoric species. Chilson et al. [1996] take a mass number of 40 which lies between that of Mg^+ (24) and Fe^+ (56). Using Massey's mobility equation [Massey, 1971] which is also given in Jones and Jones [1990] it was found that $K_0 = 2.5 \times 10^{-4}$ $m^2V^{-1}s^{-1}$ in N_2.

According to Mason and McDaniel [1988], when the geomagnetic field can be considered negligible, the ambipolar diffusion coefficient may be written as

$$D_a = D_i(1 + \frac{T_e}{T_i}), \tag{8.4}$$

where T_e and T_i are the electron and ion temperatures respectively. Once the meteor trail forms, the electrons and ions rapidly come into thermal equilibrium and as such $D_a = 2D_i$ [Cervera and Reid, 2000]. Jones [1995] has shown that electrons and ions come into thermal equilibrium within 10 collisions, which has a corresponding time of 10μs at 80 km to around 1 ms at 110 km. These times are quite short in comparison to the echo decay times measured by the radars. If we combine (8.2), (8.3), and (8.4) we may

write an expression for the ambipolar diffusion coeffiecient D_a in terms of atmospheric temperature and pressure as follows

$$D_a = 6.39 \times 10^{-2} \frac{T^2}{p} K_0. \tag{8.5}$$

Solving for T yields

$$T = \sqrt{\frac{D_a P}{6.39 \times 10^{-2} K_0}}. \tag{8.6}$$

Using diffusion coefficient data measured by the meteor radar along with an appropriate pressure model or pressure data we may solve (8.6) for T directly. In the absence of a suitable pressure model or pressure data, we can solve for the quantity $T/\sqrt{p}$ as per Tsutsumi et al. [1994] or Cervera and Reid [2000]. Note that the relationship was incorrectly published in Tsutsumi et al. [1994] as $D_a \propto T^{1/2}/\rho$ where $\rho \propto p$.

8.2 Atmospheric Pressure Models

Two independent atmospheric pressure models were used for the estimation of meteor temperatures at Davis Station, while only a single model was available for BP and Darwin. The first model was derived from AURA MLS pressure data. A brief description of satellite observation techniques can be found in Section 2.6. The AURA MLS data was provided courtesy of Dr Andrew Klekociuk of the Australian Antarctic Division (AAD). The AURA data is version 2.2 and was provided in IDL save file format for each location. The data were gridded to a 1 km resolution in geometric height coordinates. The second pressure model was developed from Falling Sphere measurements; see Section 2.7 for a brief description of the technique. Measurements were made at a latitude of 69° North which is a conjugate latitude for Davis Station. Lübken and von Zahn [1991] and Lübken [1999] have published the results in tabular format of atmospheric temperature and density as a function of geometric height from the falling sphere measurements conducted during their respective periods. Atmospheric pressure could be calculated using $p = \rho RT$ where, ρ is atmospheric density, R is the specific gas constant for dry air (287 J.kg^{-1}.K^{-1}) and T is temperature. The data provided in the Lübken papers was not entirely complete for all the required heights and times. This was especially true at the end points of the data sets. For the

density data, an exponential function was fitted to the existing height-range data such that the missing values for the upper heights could be computed for alternate months. For the temperatures a quadratic expression was fitted to the data over the height range where there was a clear turning point present in the available data. The remaining end data points for the height range were computed using the derived expressions. Once there were enough data points to provide a reliable interpolation result, the data were then read into IDL and interpolated to 365 days. Data were available for AURA MLS for 2006 and 2007 to synthesize the AURA pressure model, however the Lübken model needed to be synthesized from data recorded in 1991 and 1999. Daily averages were chosen due to the limited temporal resolution of the AURA and Lübken data. A harmonic fit was applied to the Lübken data using annual, semi annual and terannual periods. The result from the fit was used to create the Lübken pressure and temperature models and were verified against the available data in Lübken et al. [2004].

In order to compare temperatures and create an appropriate pressure model, the data was gridded to a 2 km resolution using a weighted averaging on and about the even height bin. For example, at 80 km, the data from 79, 80 and 81 km were used for the 80 km weighted average bin as follows

$$Y(z') = 0.5Y(z) + 0.25(Y(z-1) + Y(z+1)) \tag{8.7}$$

where z' denotes the new geometric bin height, z is the original even geometric height and Y is the data at that height. A graphical representation of the weighting function can be seen in Figure 8.1. The concept was to create an artificial pulse smearing effect that is similar to the pulse smearing that occurs with meteor radar observations in order to increase the similarity of the techniques used between data sources.

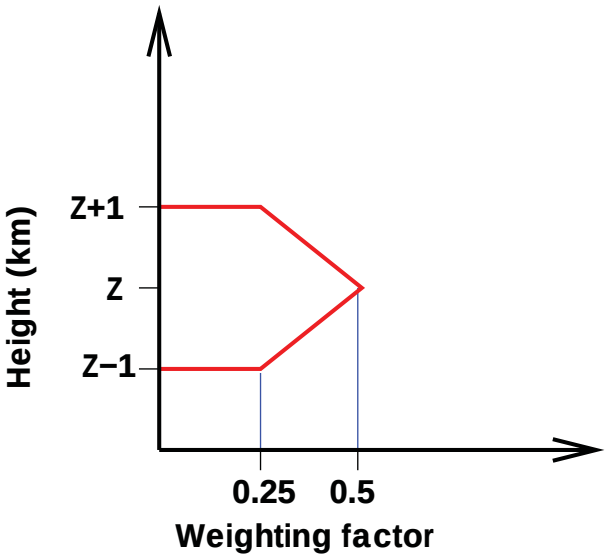

Figure 8.1: Weighting function applied to AURA and Lubken data in order to semi-synthesize the pulse smearing effect associated with meteor radar observations.

8.3 Davis Temperature Comparisons

Using the Davis 33.2 MHz and 55 MHz diffusion coefficient data along with AURA and Lübken based pressure models we were able to generate temperature estimates on and about the peak height of the meteor distribution. In theory (8.6) should allow us to calculate temperature estimates from meteor data across the entire meteor height distribution subject to us having a suitable pressure model and enough echoes to provide an accurate estimate of the mean diffusion coefficient. This method is in contrast to that of Hocking et al. [2004] who use the so-called "temperature gradient" technique. This involves performing the regression analysis outlined in Section 7.1.1 on a plot of $\log_{10} D_a$ and height to determine the slope of the relation between the two quantities, along with estimating the temperature gradient of the atmosphere at a particular height. For the pressure model technique, height and diffusion coefficient errors along with geophysical variations in the diffusion coefficient estimates can bias the results of the mean diffusion coefficient estimated at a particular height [Hocking et al., 1997, Holdsworth et al., 2006]. Figure 8.2 shows the variation in the peak height of the meteor distribution for both the

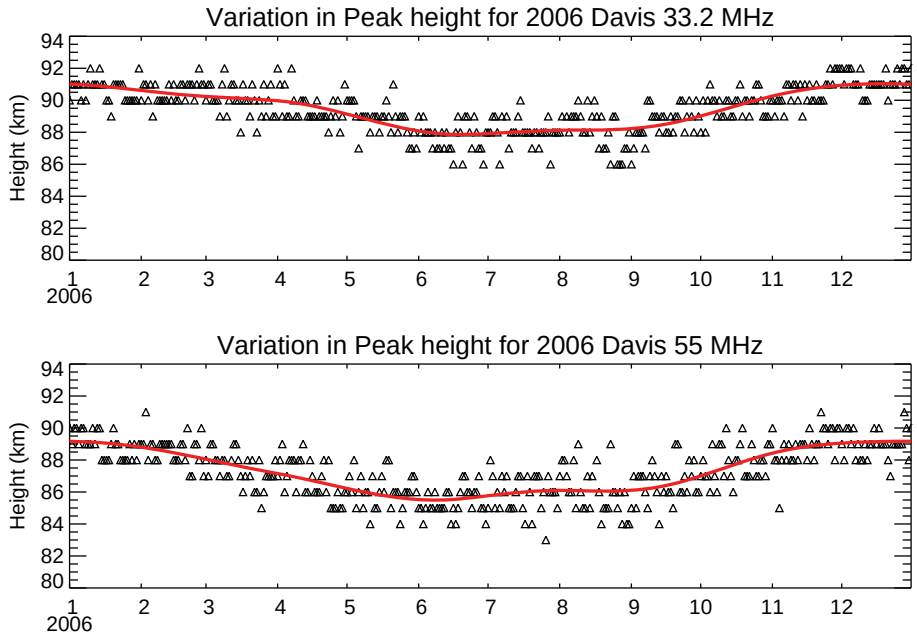

Figure 8.2: 2006 Davis 33.2 and 55 MHz Meteor radar variation in the height of the peak of echo detections. The solid red line represents a harmonic fit to the data using annual (365 days), semiannual (182.5 days) and terannual (120 days) periods.

33.2 MHz and 55 MHz meteor radars. As such, a compromise peak height of 90 km was selected for the comparison of temperatures initially.

The satellite observations were two points in the day separated by approximately 12 hours corresponding to a day time and an evening time pass of the satellite. Due to the limitation of the number of satellite observations in a 24 hour period, effective daily averaged temperature and pressure were calculated for the satellite observations. Meteor diffusion coefficients for each day were averaged using an outlier rejection method with a 2.5 standard deviation rejection criteria. These were subsequently used to calculate daily averaged meteor temperature estimates for comparison. In the process of creating the daily averages for both the satellite and meteor data, the effective time points to which both the satellite and diffusion coefficients average to only differ by a couple of minutes. As such, the phase error in comparing the two can be considered to be negligible in comparison to other sources of error. Data from 2006 and 2007 for both meteor radars were made available

thanks to Dr Damian Murphy from the AAD. The pressure model derived from the AURA MLS observations along with the diffusion coefficient data was used to generate the temperature estimates which can be seen in Figure 8.3.

Given the similarities between the temperature estimates and variation of the 2006 and 2007 data, the following comparisons presented are using 2006 data. The results from 2007 are very similar to those of the 2006 data and thus offer no further insight. There is an un-accounted for offset to the 33.2 MHz meteor temperatures of approximately 30 K which is present at Davis and can be seen in Figure 8.3. Both meteor temperatures however exhibit similar features despite the offset. The temperatures determined using the 33.2 MHz data at 90 km are similar to the results obtained by Hall et al. [2004] and Hall et al. [2006] where pressure models were derived from CIRA86, MSIS-90, MSIS-00 and the work of Lübken and von Zahn [1991] at a constant height of 90 km.

A more rigorous means of comparing the temperatures is to apply the regression analysis technique outlined in Section 7.1.1. To do this we first subtract the respective mean temperatures from the temperature data sets. By inspection of Figure 8.4 we can see that both the 33.2 MHz and 55 MHz meteor temperature estimates exhibit similar features in terms of their annual and semiannual oscillations. By inspection we can also see that there is also greater variance on a day-to-day basis with the 33.2 MHz estimates compared with both the AURA and 55 MHz estimates. We consequenty generate a scatter plot for a particular height (see Figure 8.5) and calculate the corresponding statistical quantities which are summarised in Figures 8.6 and 8.7. The effects of anomolous diffusion as discussed by Dyrud et al. [2001] and Hall [2002] have been noted and the results of the temperature comparisons outside the peak height are presented for completeness. The regression analysis results of both the 33.2 MHz and 55 MHz meteor temperature estimates show a high correlation over a significant height range. This can be attributed to the variation in the peak height of the meteor distribution which as has been observed is as much as approximately half a scale height ($\sim$3.6 km). This would also explain why there is better agreement between the meteor temperature estimates at certain points of the year as opposed to others.

Holdsworth et al. [2006] demonstrated the importance of evaluating meteor temperatures at the peak height of the meteor distribution as opposed

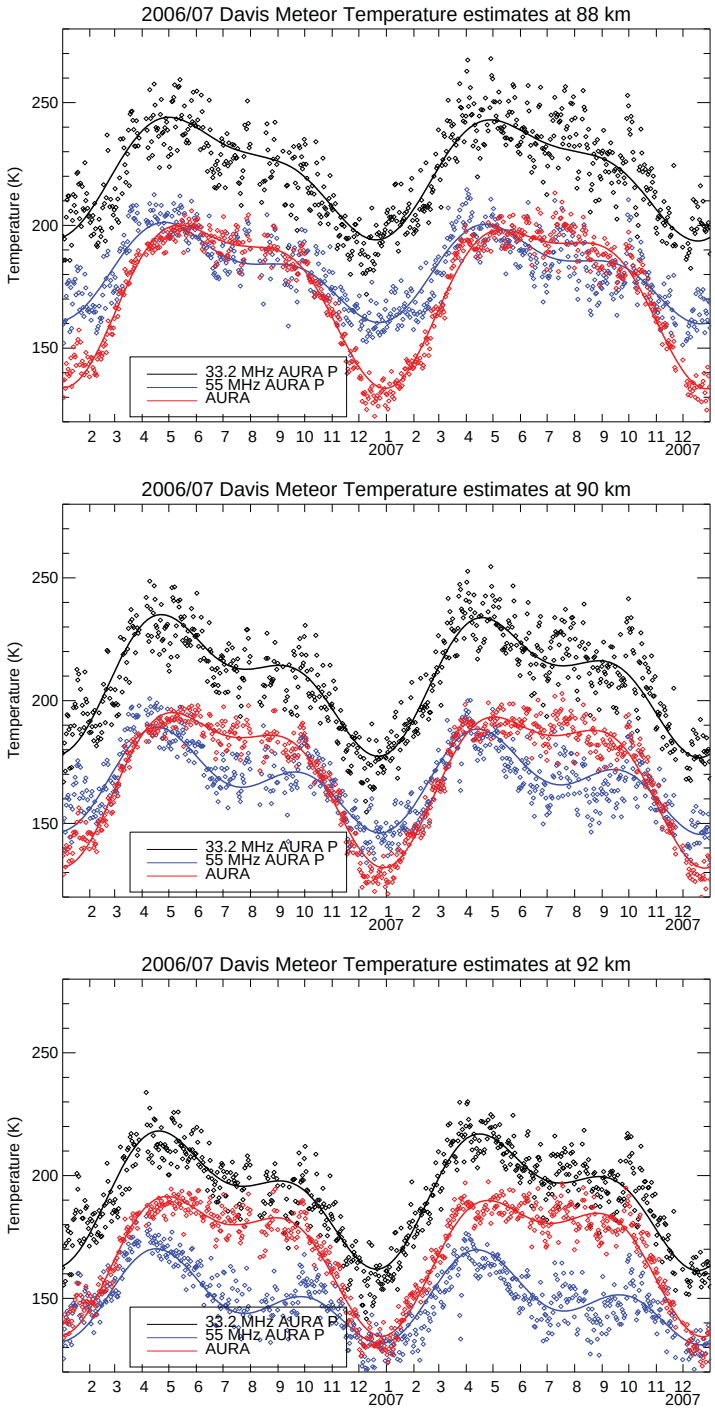

Figure 8.3: Davis 2006/07 meteor and AURA MLS daily temperatures. The diamonds indicates the raw data points and the solid lines represent harmonic fits to the data sources using annual, semiannual and terannual periods.

to a constant height. The pressure model developed by Holdsworth not only incorporated the temporal variation of atmospheric pressure, but the variation in the peak height of the meteor distribution. Along with evaluating the mean diffusion coefficient at the peak height, this allowed for the best estimate of average diffusion coefficient and hence temperature estimate based upon Holdsworth's derived pressure model.

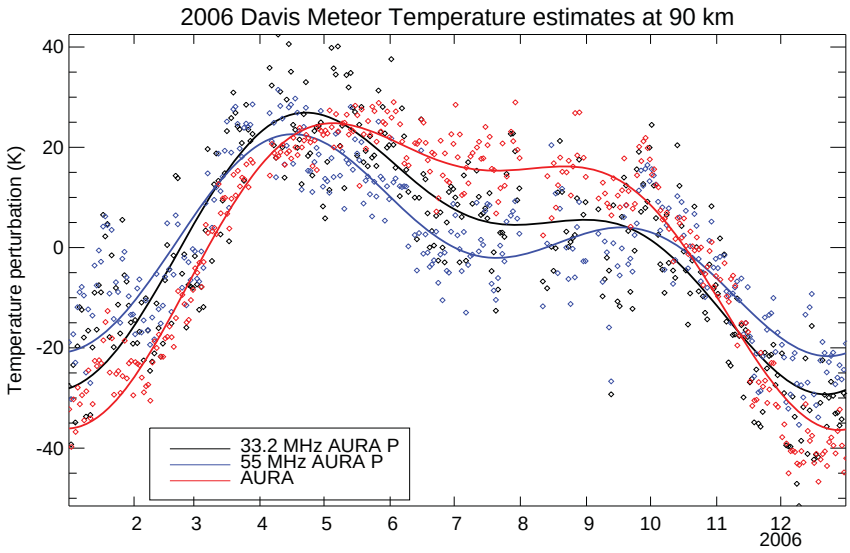

Figure 8.4: Davis 2006 meteor and AURA MLS daily temperature perturbations about the mean. The diamonds indicates the raw data points and the solid lines represent harmonic fits to the data sources using annual, semiannual and terannual periods.

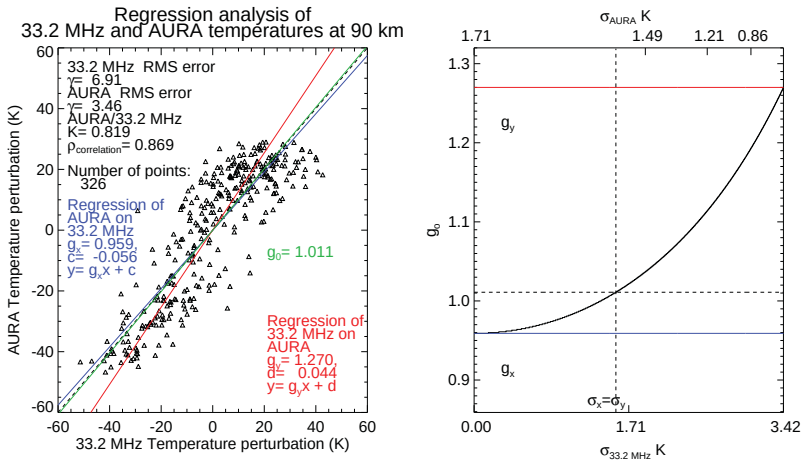

Figure 8.5: Davis 2006 meteor and AURA MLS daily temperature scatter plot.

In order to verify the quality of the meteor temperature estimates and how much they are influenced by the small scale fluctuations present in the AURA pressure model, a second pressure model was synthesised from the Lübken data [Lübken and von Zahn, 1991, Lübken, 1999], which is what the Holdworth pressure model was created from [Holdsworth et al., 2006]. The Lübken model was also used to attempt to explain the offset present in the 33.2 MHz meteor temperatures. The meteor temperatures were re-calculated using the Lübken pressure model and can be seen in Figure 8.9 along with the meteor temperatures derived using the AURA pressure model. OH temperatures represent a weighted average over the emission layer and the height of the distribution varies through the course of the year [Kumar et al., 2008]. As such a mean height of 88 km was selected for Davis Station. 88 km also represents a mean height for the meteor distributions and hence comparisons made between meteor and OH temperatures are made at this height. Initially OH data was sourced from French et al. [2005] which represented an 8 year climatological mean. The harmonic fit for the OH data in Figure 8.9 represents a 13 year climatological mean of the observations made between 1995 and 2007. This can be seen as the purple line with no data in the southern hemisphere summer months. This data was provided by Dr John French of the AAD through private correspondence. The end points of the interpolation are not reliable due to the interpolation becoming unbounded

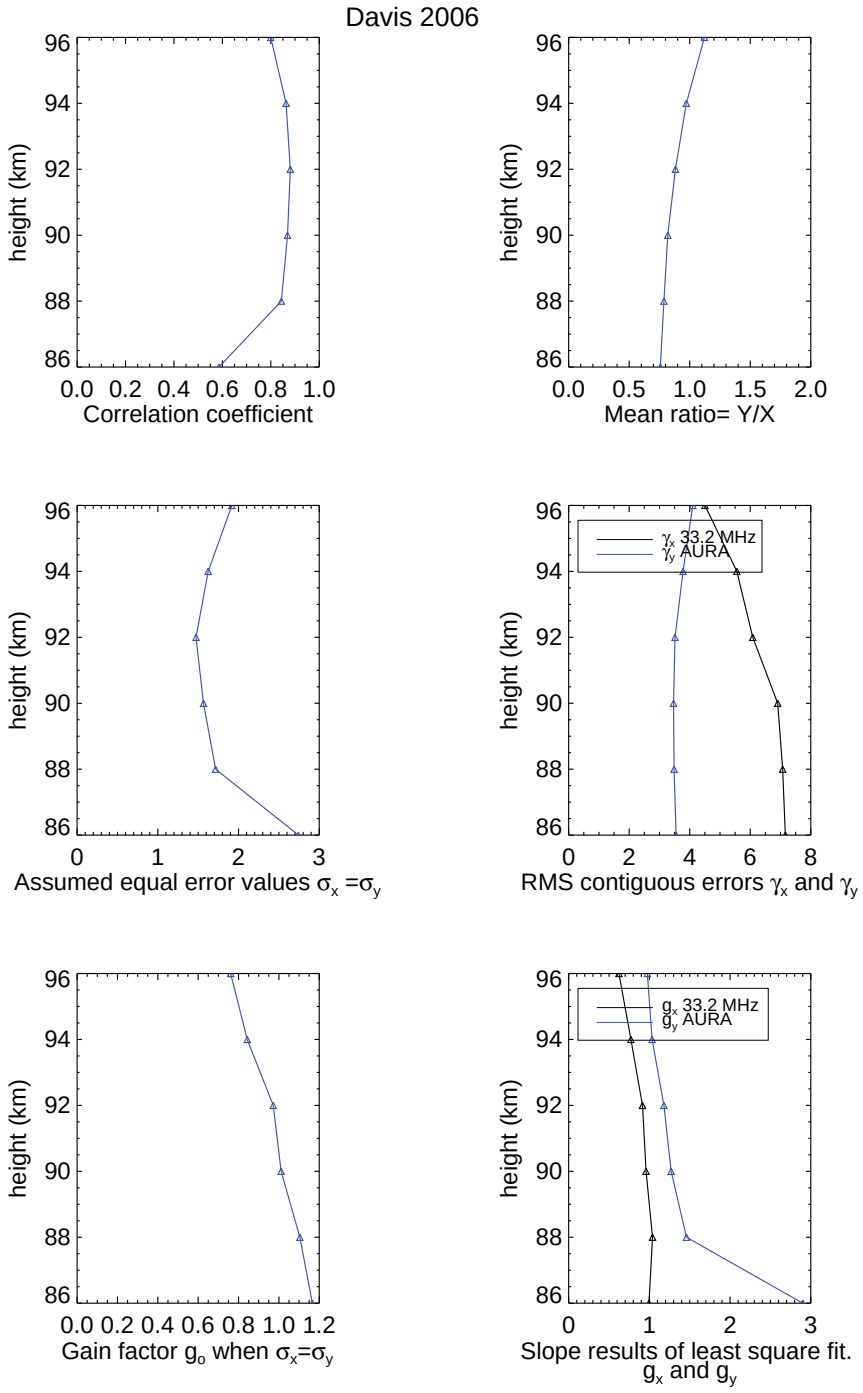

Figure 8.6: Davis 2006 33.2 MHz meteor and AURA MLS daily temperature regression results. Meteor temperatures derived using AURA pressure model.

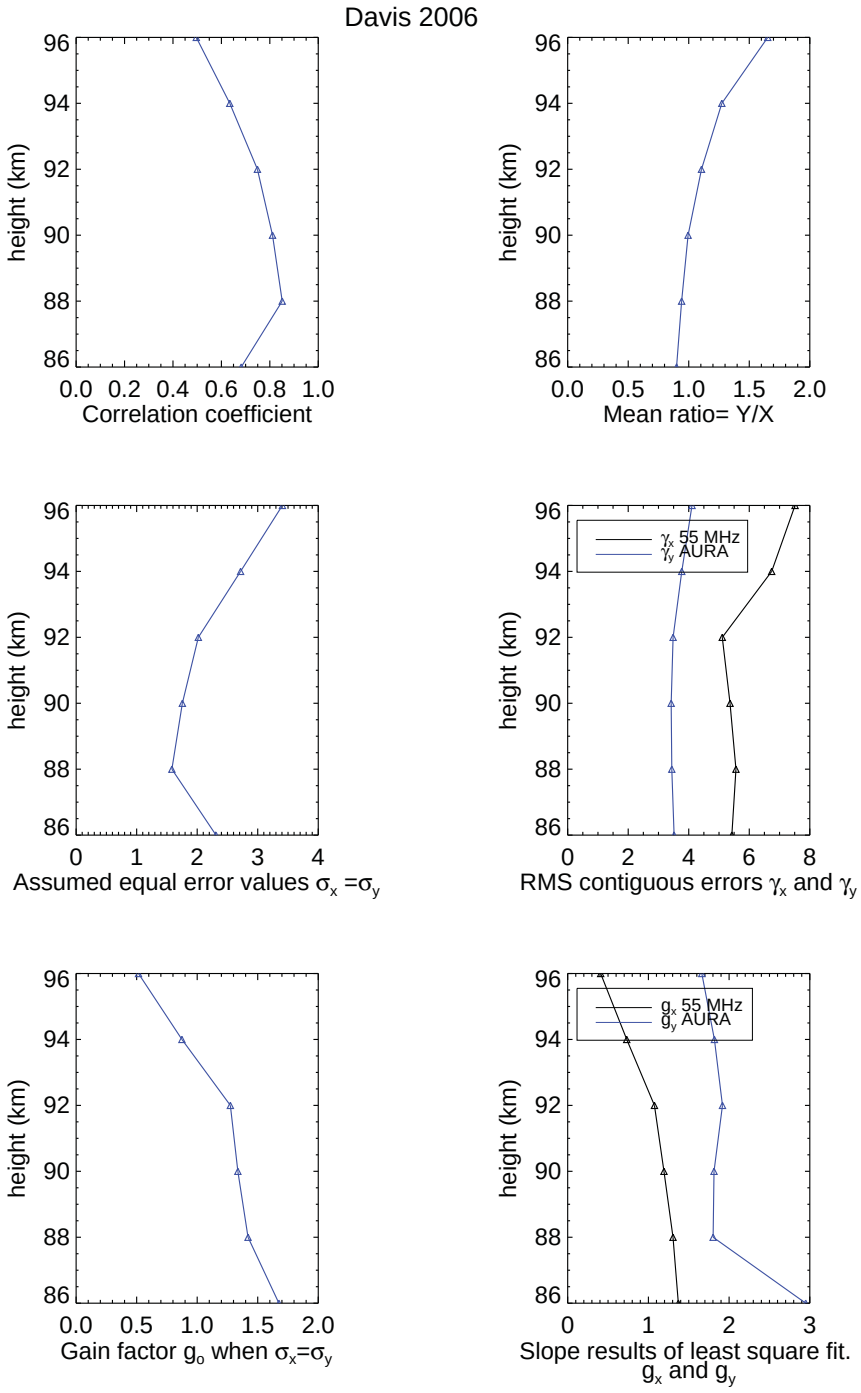

Figure 8.7: Davis 2006 55 MHz meteor and AURA MLS daily temperature regression results. Meteor temperatures derived using AURA pressure model.

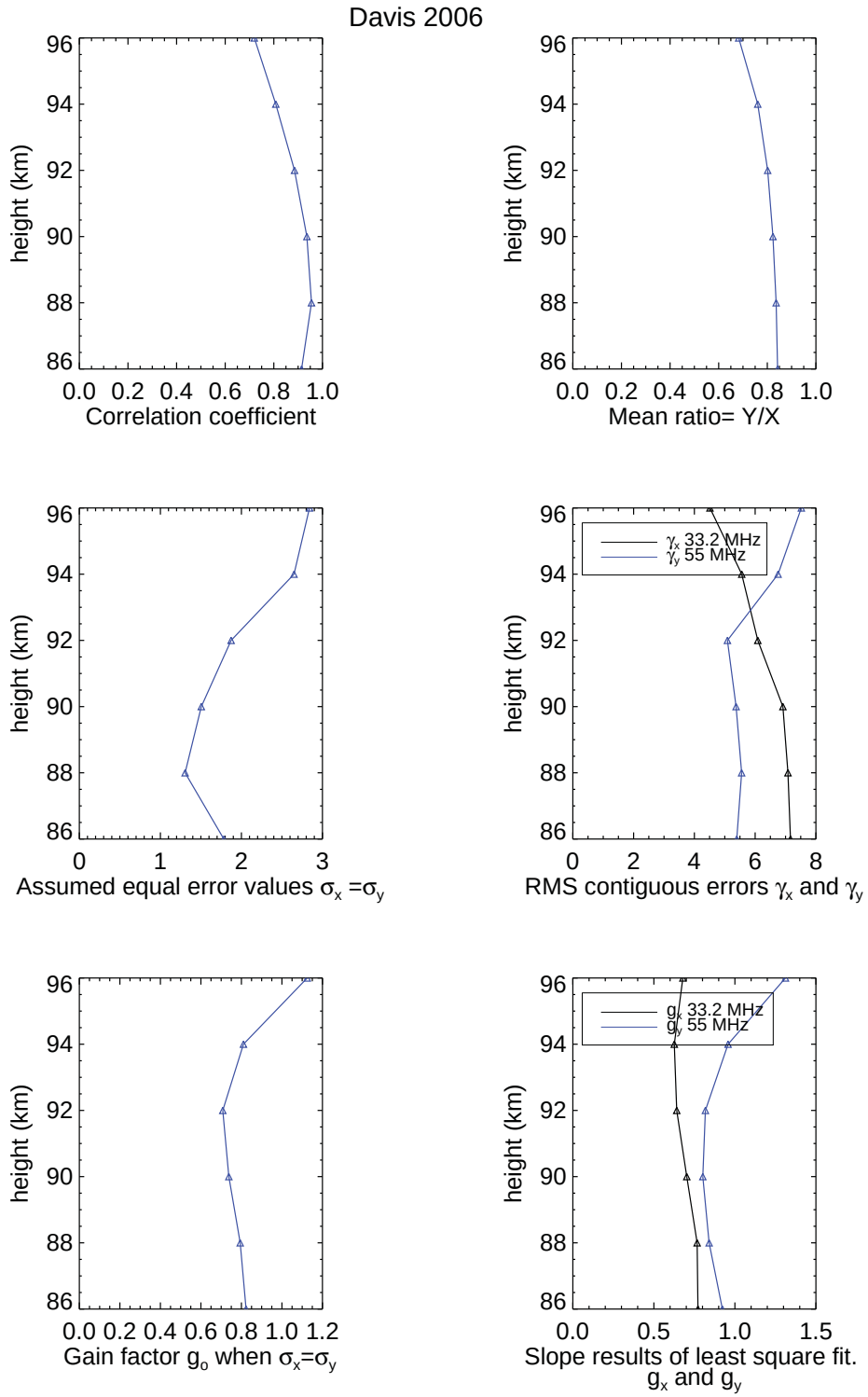

Figure 8.8: 2006 Davis 33.2 MHz and 55 MHz meteor scatter statistics summary.

due to no available data during the summer (all daylight) months at Davis. We can clearly see that the 33.2 MHz temperature estimates still exhibit an approximate 30 K offset from the 55 MHz and AURA temperatures regardless of the pressure model used. The 55 MHz temperatures derived using the AURA model along with the AURA temperatures are slightly cooler than the Lübken based meteor and OH temperatures. According to Froidevaux et al. [2006] AURA MLS temperatures are generally cooler when compared with other measurements, and this is consistent with the observations made here. Shepherd et al. [2004] published a table of mean values and amplitudes for temperatures measured at various latitudes. When the data in the table is interpolated to 69°, the AURA based 55 MHz meteor temperatures in Figure 8.9 are comparable in amplitude and mean value to those of the WINDII results.

8.3.1 Comparison of Temperatures at the Peak Height

If we follow the method of Holdsworth et al. [2006] and compare the temperatures at the peak height of the meteor distribution (accounting for its variation) as opposed to a constant geometric height (e.g. Hocking et al. [1997], Hall et al. [2004]), we find that there is in fact more consistent agreement throughout the year between the meteor temperature estimates and other sources. Figures 8.3 and 8.9 show meteor temperature estimates at constant geometric height. We observe, particularly in Figure 8.3, the deviation of the meteor temperature estimates from those of other sources at different points in the year. If we select the temperature estimates at the peak height throughout the year for comparison, we observe a more consistent agreement throughout the year, particularly with the 55 MHz temperatures. The 33.2 MHz temperatures, however, still exhibit the 30 K offset (see Figure 8.10). By evaluating the temperatures at the peak height, we subsequently minimise the ambiguity introduced into the mean diffusion coefficient estimates from geophysical phenomena outside the peak height, thus producing more reliable temperature estimates. Correlation coefficients were calculated for the data sets. The maximum correlation value obtained between data sets at constant geometric height was approximately 0.85. The correlation values obtained by comparing temperatures at the peak were typically greater than 0.91 which suggests that evaluating the temperature at the peak height is the best approach. The Lübken based 55 MHz meteor temperatures ex-

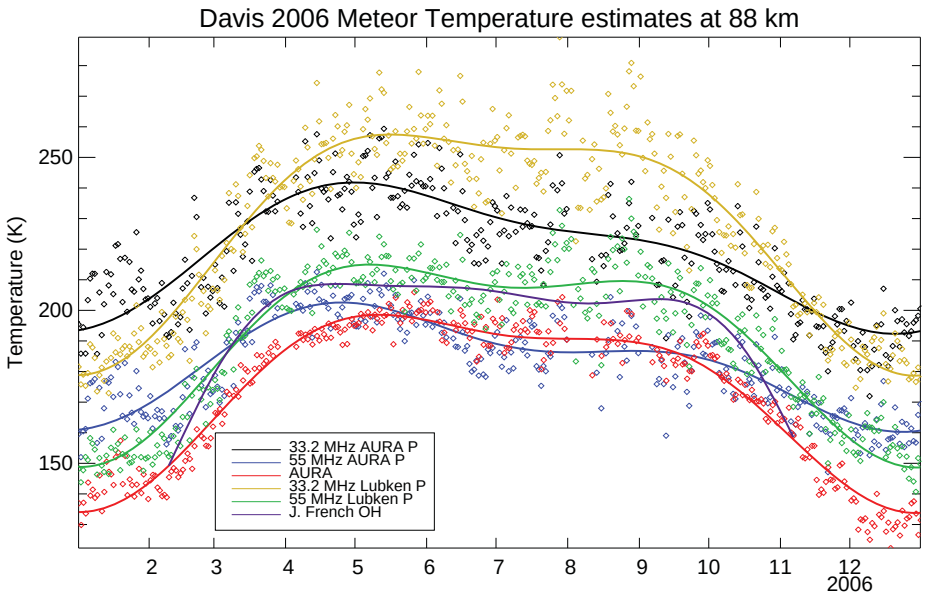

Figure 8.9: 2006 Davis 33.2 MHz and 55 MHz meteor temperatures derived using AURA and Lübken pressure models. The diamonds indicates the raw data points and the solid lines represent harmonic fits to the data sources using annual, semiannual and terannual periods. The black and yellow curves represent the 33.2 MHz meteor temperatures estimated using AURA and Lübken pressure models respectively. The blue and the green represent the 55 MHz meteor temperatures using AURA and Lübken pressure models respectively. The red curve represents AURA MLS temperatures and the purple represents the results from the John French OH harmonic fit to Davis OH data.

hibit an amplitude of approximately 80 K, which is consistent with what was found by Holdsworth et al. [2006], however the 55 MHz meteor temperatures in this study have a mean value of approximately 180 K compared with approximately 170 K found in Holdsworth et al. [2006]. The next section investigates what the role of strong and weak meteor echoes have in the determination of temperature estimates.

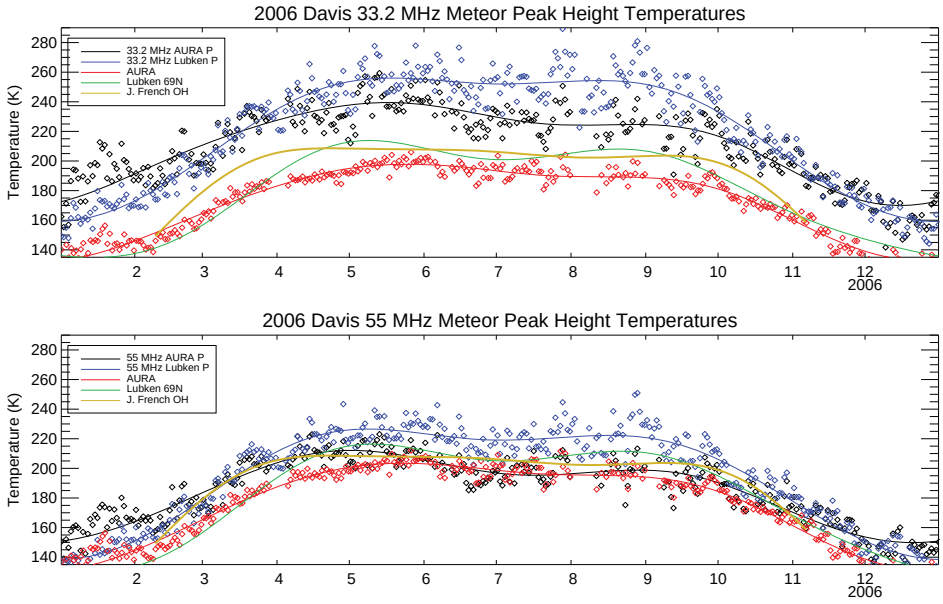

Figure 8.10: 2006 Davis 33.2 MHz and 55 MHz meteor peak height temperatures derived using AURA and Lübken pressure models. The diamonds indicate the raw data points and the solid lines represent harmonic fits to the data sources using annual, semiannual and terannual periods. The OH temperature fit is provided for comparison as the OH temperature estimates are at or within 1 km of the peak height during the course of the year. The Lübken temperatures are provided as another reference source. The Lübken temperatures are cooler than the AURA temperatures at the beginning of the year (these are known to be on the cold side), which would suggest that these temperatures are not ideal for comparison at these times. The Lübken temperatures do however show reasonable agreement with the French OH temperatures during the course of the year.

8.3.2 Strong and Weak Echo Temperatures

According to Younger et al. [2008], estimates of meteor diffusion coefficients may be adversely affected by the presence of aerosols and ice crystals which may nucleate on dust particles. Evidence of this can be seen in the development of Polar Mesospheric Summer Echoes (PMSE). Depending upon the radar frequency of observation, the presence of these aerosols and ice crystals can lead to either a reduction or an increase in the decay time measured for a particular echo with a particular line charge density. From (8.1) it is evident any variation to the decay time will consequently effect estimates of the diffusion coefficient and thus temperature estimates. The echo segregation procedure involved finding the median SNR value for all meteor detections without a priori knowledge of the distribution of SNR values, nor the exact correspondence between SNR values and electron line densities for the trail. The relation between SNR and line density for each radar could be established using the results from the method outlined in Section 6.2. The data set was subsequently split about the median point with echoes with SNR less than the median value defined as weak and those with SNR greater than the median defined as strong. For the range of SNR values observed, refer to Table 8.1. The procedure was subsequently repeated for the strong and weak data sets to obtain the strongest and weakest echoes. Assuming that the distribution of SNR of meteor detections is evenly distributed from minimal detectable SNR to maximum SNR capable of being measured by the receivers, this would result in the two final data sets representing the strongest and weakest 25 percent of all echoes detected. Furthermore, following the results of Section 8.3.1 we restrict our estimates to the peak height. The results can be seen in Figure 8.11.

From the results in Figure 8.11, we find that by taking the strongest echoes for the 55 MHz system, we obtain the temperature estimates which exhibit strong agreement with both the AURA MLS and Lübken temperatures, however the 33.2 MHz estimates exhibit the characteristic 30K offset which is present in the previous temperature estimates. The strong echo AURA based 55 MHz temperatures are $\sim$20 K warmer and show 10 K less in amplitude than those of Holdsworth et al. [2006]. This could be due to Holdsworth et al. [2006] incorporating strong and weak echoes in the temperature estimates or possibly due to the 55 MHz meteor radar having less observation time as a result of PMSE experiments that are run during the

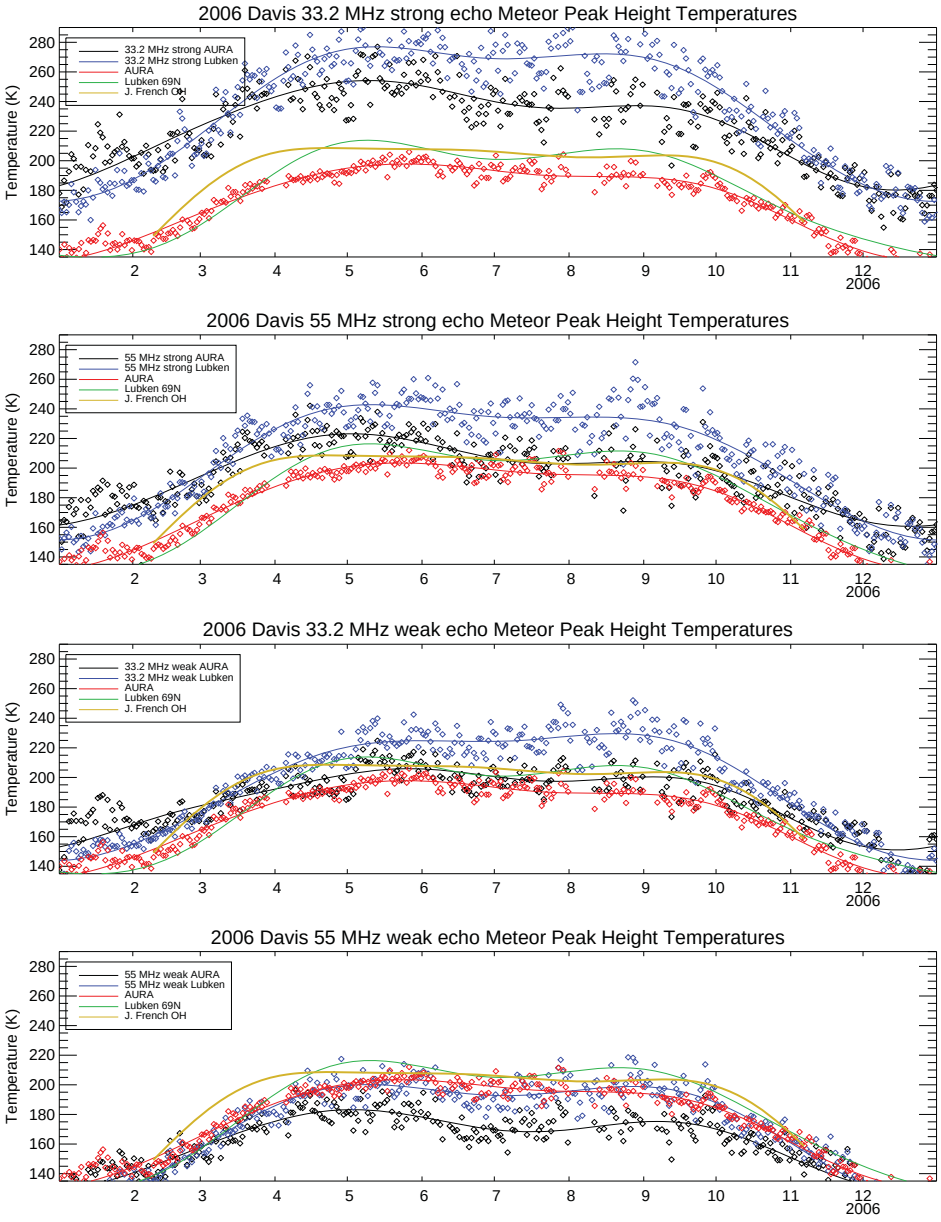

Figure 8.11: 2006 Davis 33.2 MHz and 55 MHz strong and weak meteor echo temperatures at the peak height derived using AURA and Lübken pressure models. The diamonds indicates the raw data points and the solid lines represent harmonic fits to the data sources using annual, semiannual and terannual periods. The OH temperature fit is provided for comparison as the OH temperature estimates are at or within 1 km of the peak height during the course of the year.

Location and System	Minimum SNR (dB)	Maximum SNR (dB)
Davis 2007 33.2 MHz	7.28	75.28
Davis 2007 55 MHz	9.00	96.80
Darwin 2007 33.2 MHz	8.74	79.33
BP 2006 55 MHz	9.18	53.27

Table 8.1: The minimum and maximum observed SNR values for meteor echoes detected by the systems used within this study. The figures were provided via private correspondence by Joel Younger from the Atmospheric Physics Group, University of Adelaide.

summer months at Davis. The temperature estimates in the weak case are slightly cooler than the AURA and Lübken counter parts, but the 33.2 MHz temperature estimates exhibit a much better agreement with the AURA and Lübken temperatures. The results from the temperature estimates appear to support the conclusions of Younger et al. [2008]; however the model predictions can not be completely verified without having knowledge of the relation between SNR values and electron line density. Correlation coefficients were calculated between both AURA and Lübken based meteor temperatures and AURA and Lübken temperatures. It was initially thought that temperatures estimated with strong meteor echoes would provide higher correlation values compared with those estimated using weaker echoes. This in fact turned out not to be the case. The offset which is present in the strong echo 33.2 MHz estimates proved to have no significant impact on the correlation result. This was evident by the fact that the correlation value obtained was similar to the value obtained for the weak 33.2 MHz echo temperature estimates which exhibited approximately the same mean value as the AURA and Lübken temperature estimates. It should also be noted that the there is no direct relation or correspondence between SNR values measured between the 55 MHz and 33.2 MHz systems. Each of the systems operate using different receiver bandwidths and each system is susceptible to different background noise sources, thus producing completely different noise floors and receiver temperatures to which SNR values are determined with respect to. In the next section we apply the same quality control restrictions of peak height variation and strong and weak echo classification to analysing meteor temperatures generated with the BP meteor radar.

8.4 Buckland Park Temperature Comparisons

Temperature estimates were derived using the 2006 diffusion coefficient data from the BP high-powered meteor radar system along with a pressure model derived from AURA pressure data. There was limited data available for 2007 due to the constant refinement of the system and the results using the data available showed little variation from the results using the 2006 data and as such are not presented. Another source of temperature measurements were SABER satellite observations provided by Dr Rolando Garcia from the Atmospheric Chemistry Department (ACD) of the National Center for Atmospheric Research (NCAR), Boulder Colorado. The SABER data provided for both BP and Darwin locations were an early revision of the data. The data were prepared to 4° latitudinal and 5° longitudinal resolution. The data points were in 2 passes per day; one at 0:00 UT and the second at 12:00 UT. The vertical resolution of the data was approximately 3 km in pressure height coordinates. The SABER data was converted to daily averages and the pressure heights converted to geometric heights by multiplying by an approximate scale height of 7 km. The data was subsequently interpolated to a regular even geometric height grid with a resolution of 2 km. The AURA data was prepared in the same manner as it was for the Davis comparisons.

Initially temperature estimates were calculated at constant geometric heights along with certain statistical quatities. The statistical quantities were determined using the same methodology used with the Davis data. The results can be found in Appendix D. Following the results of the Davis temperature comparisons, meteor temperatures were estimated at the peak height. The variation in peak height can be seen in Figure 8.12. Figure 8.13 shows there is in fact good agreement during the course of the year between the meteor temperature estimates and both AURA and SABER temperatures, however the summer (Southern Hemisphere) period shows good agreement between the meteor and AURA but not with the SABER temperatures. The meteor, AURA and SABER temperatures show comparable mean temperatures during the course of the year, however the correlation between the SABER and meteor data sets was found to be quite low compared with the AURA and meteor correlation values (see Appendix D). The meteor temperatures are approximately 10 K cooler than the AURA. From the observations made with the Davis temperature estimates at 55 MHz, it

was observed that weaker echoes introduce a bias into the average diffusion coefficient that results in cooler temperature estimates. The meteor data was subsequently divided up into the strongest and weakest echoes utilising the same segregation technique outlined in Section 8.3.2. The daily average diffusion coefficient was re-calculated and temperatures re-estimated. The results can be seen Figure 8.14. The yellow line represents the harmonic fit result to OH temperatures derived in the working manuscript of Iain M. Reid, Jonathan M. Woithe, and G.G. Sivjee entitled *Observations of TOH and TO2 temperatures at Adelaide, Australia*. The amplitude and phase parameters were provided by Professor Reid from the School of Chemistry and Physics, University of Adelaide, through private correspondence. The purple line was generated using the harmonic fit results to OH temperatures published in a paper by Gelinas et al. [2008] with a correction to the tabled semiannual amplitude component as suggested by Reid. From Figure 8.14, it is clear that temperatures derived using the stronger echoes show better agreement during the course of the year, however the temperatures derived during the summer months are cooler than AURA, both OH temperature fits and SABER temperatures. It can be seen in Figure 8.14 that during the course of the year all temperature estimates are within approximately $\pm$ 5 K of the mean temperature of approximately 192 K. This result is also in strong agreement with those found by Shepherd et al. [2004] in the WINDII experiment at 35° S. It is clear from the blue curve in Figure 8.14 that the use of weak echoes leads to lower temperatures estimates and would serve to explain the offset present in the meteor temperatures in Figure 8.13.

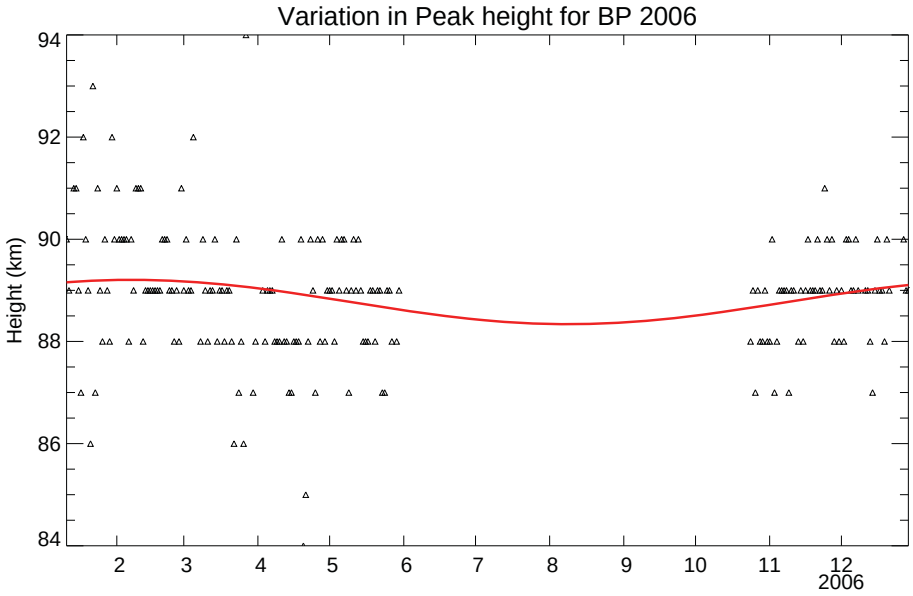

Figure 8.12: 2006 BP 55 MHz Meteor radar variation in the peak height of the echo detections. The solid red line represents a harmonic fit to the data using only an annual (365 days) period. Initially semiannual and terannual periods were fitted but it was found that the gap in the observations artificially enhanced the amplitude results for those periods in the harmonic analysis.

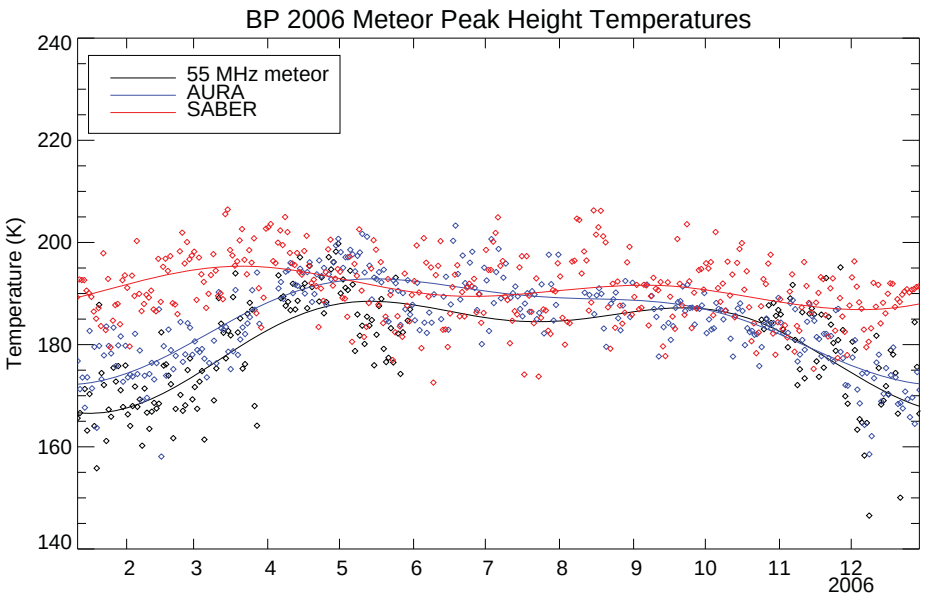

Figure 8.13: 2006 BP 55 MHz Meteor radar peak height temperature estimates with AURA MLS and SABER temperatures. The solid lines represent a harmonic fit to the data using annual (365 days) and semiannual (182.5 days) periods. The diamonds represent the original daily temperature estimates.

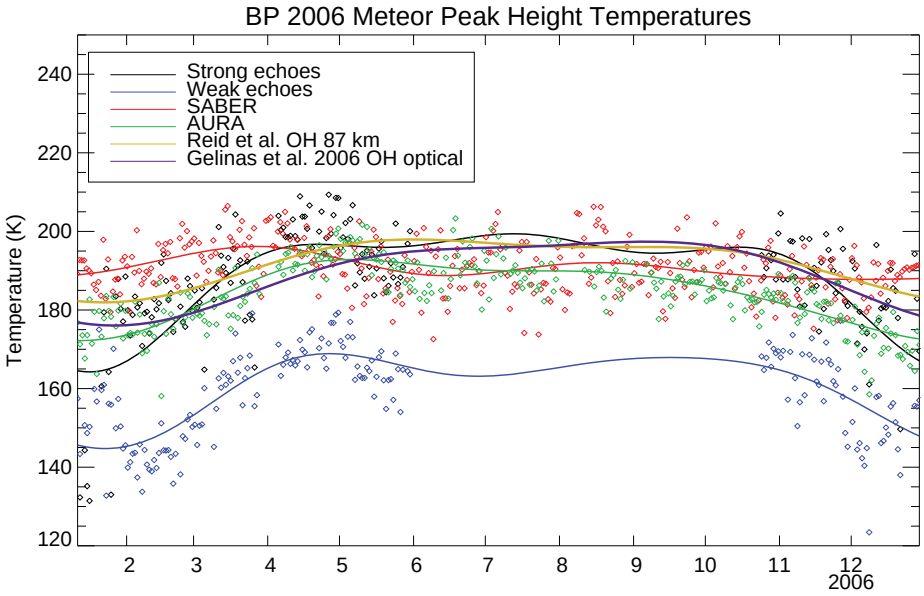

Figure 8.14: 2006 BP 55 MHz Meteor radar peak height temperature estimates using strong and weak echoes with AURA MLS and SABER temperatures. The solid lines represents a harmonic fit to the data using annual (365 days) and semiannual (182.5 days) periods. The diamonds represent the original daily temperature estimates.

8.5 Darwin Temperature Comparisons

Temperature estimates for the Darwin 33.2 MHz system along with AURA and SABER data were derived using the same methodology as used for both the BP and Davis analysis. Temperature estimates were determined at a constant geometric height and associated statistical quantities calculated. See Appendix D. As with the BP temperature estimates, the mean temperatures are comparable between the three data sets, however the correlation between the meteor and SABER temperatures is lower than the correlation between the AURA and the meteor temperatures. The meteor data was sorted into strong and weak echo classification and temperatures were subsequently determined at the peak height of the meteor distribution. Given Darwin's latitude there is no real variation in the peak height as shown by Figure 8.15. An interesting point to note is the lack of the 30 K offset which is present in the Davis 33.2 MHz temperature estimates, which would seem to imply there could in fact be a latitudinal effect present in measurements of the diffusion coefficient with the 33.2 MHz system. The initial peak height temperature estimates can be seen in Figure 8.16. Figure 8.17 shows the results from the separation of the echoes into strong and weak echo classification and re-estmation of temperatures using the two classes of echoes. Shepherd et al. [2004] found a mean temperature at 10° of approximately 192 K with an amplitude of 1.3 K. The meteor temperatures in Figure 8.17 have a mean temperature of approximately 185 K and a amplitude variation of close to 20 K. It should be noted that the peak height of the meteor distribution never dropped below 90 km and as such the meteor temperatures at the peak height should be expected to be slightly cooler than those of the WINDII temperatures which were mapped to 87 km. The SABER temperatures in Figure 8.17 show a mean temperature of approximately 190 K with very little amplitude variation during the course of the year which is more in agreement with the WINDII results. As with all the other meteor temperature comparisons it is evident that weak echoes serve to bias meteor temperature estimates and provide cooler temperature estimates.

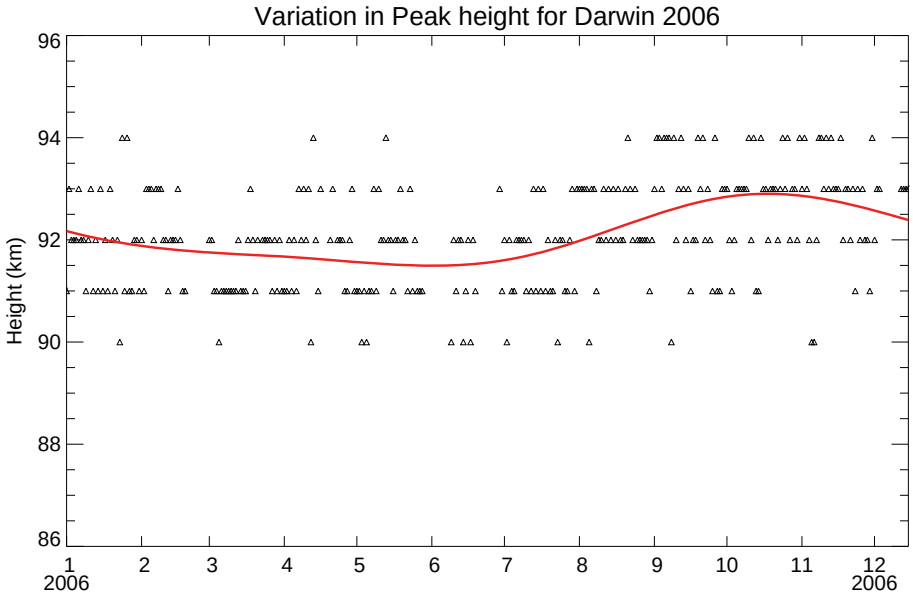

Figure 8.15: 2006 Darwin 33.2 MHz Meteor radar variation in the peak height of the echo detections. The solid red line represent a harmonic fit to the data using annual (365 days) and semiannual (182.5 days) periods.

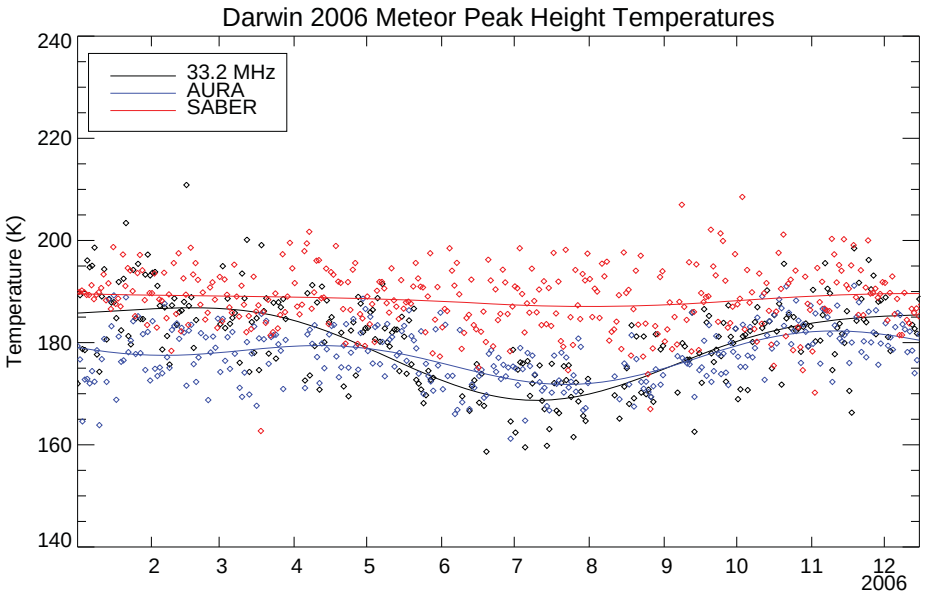

Figure 8.16: 2006 Darwin 33.2 MHz Meteor radar peak height temperature estimates with AURA MLS and SABER temperatures. The solid lines represents a harmonic fit to the data using annual (365 days) and semiannual (182.5 days) periods. The diamonds represent the original daily temperature estimates.

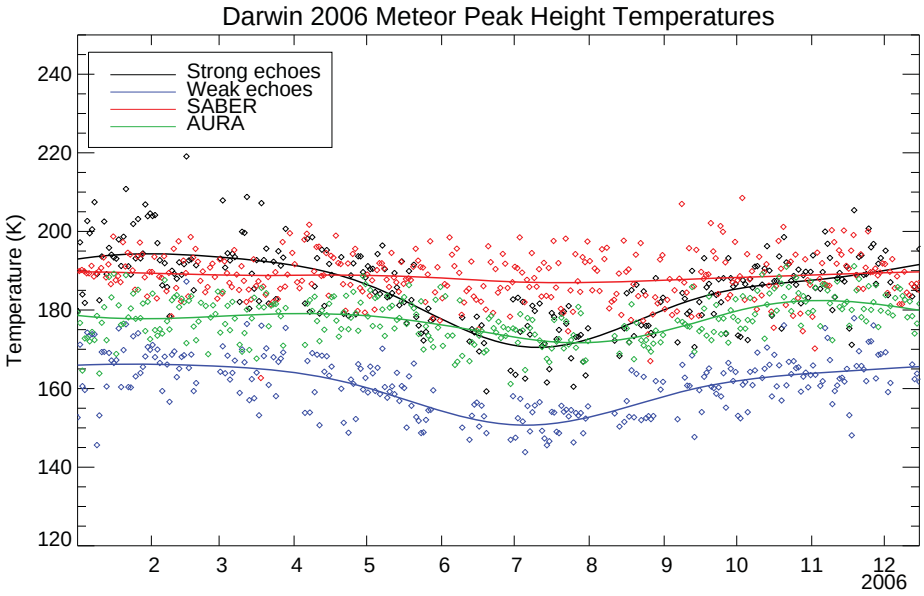

Figure 8.17: 2006 Darwin 33.2 MHz Meteor radar peak height strong and weak echo temperature estimates with AURA MLS and SABER temperatures. The solid lines represents a harmonic fit to the data using annual (365 days) and semiannual (182.5 days) periods. The diamonds represent the original daily temperature estimates.

8.6 Summary

Mesospheric temperature estimates for Davis Station, Buckland Park and Darwin were determined using meteor diffusion coefficient data in combination with an atmospheric pressure model. This technique was chosen chiefly due to its ease of implementation, however Holdsworth et al. [2006] cite the minimization of statistical errors and 'reduced occurrence of discrepancies' as further motivating factors for the use of the pressure model technique. Atmospheric pressure models were determined for each location based upon AURA pressure data. Davis Station had the additional benefit of another pressure model based upon conjugate latitude northern hemisphere falling sphere measurements of atmospheric density and temperature [Lübken and von Zahn, 1991, Lübken, 1999]. This formed the basis for the Lübken pressure model used to generate meteor temperature estimates independent of AURA data and thus allowed for investigation into the influence the pressure model has upon meteor temperature estimates. Darwin was the only location that could not be directly compared with OH observations and Davis Station could not be compared with SABER observations due to lack of data. While other comparisons of $T/\sqrt{p}$ have been performed [Cervera and Reid, 2000, Hocking et al., 1997] that offer a more independent means of comparison between meteor observations and other techniques, it was elected to generate direct temperature estimates which could be directly compared with co-located OH observations.

The atmospheric pressure models using both AURA and falling sphere data were synthesized in a manner that would attempt to incorporate the pulse smearing effects associated with the meteor radar observations. As such a weighting function was applied to the data as described by (8.7), which was applied when re-gridding the data to two kilometre height bins. Unlike the AURA data which were concurrent with the meteor observations, the Lübken pressure model was synthesized using interpolation techniques on 1991 and 1999 falling sphere data. It is evident from the results in Figures 8.9 and 8.10 that the pressure model influences the outcome of temperature amplitude and variation, however the offset observed between 33.2 MHz and other temperature estimates is independent of the pressure model chosen. A similar offset has been observed in the studies by Hall et al. [2004] and Hall et al. [2006] who have used pressure models derived from CIRA86, MSIS-90, MSIS-00 and Lübken and von Zahn [1991] observations, however no clear

explanation for the observed offset is evident form the results of this study. A regression analysis was performed on the Davis meteor temperature estimates after the mean temperature was removed as per Section 7.1.1. High correlations between meteor temperature estimates and AURA temperatures as well as meteor-meteor temperatures were found. In fact, the 33.2 MHz temperatures exhibited a higher correlation with AURA temperatures over the height range of the distribution compared with that of the 55 MHz and AURA comparison. This could possibly be attributed to a decreased number of echoes in the case of the 55 MHz observations in range bins away from the the peak and a possible greater influence from geophysical phenomena on diffusion coefficient estimates.

Temperature estimates were made initially at constant geometric height corresponding to the annual mean peak height of the meteor distribution, however following the recommendation of Holdsworth et al. [2006] temperatures were re-evaluated at the peak height of the meteor distribution which at Davis Station can be seen to vary by as much as half a scale height (See Figure 8.2). Younger et al. [2008] has shown that meteor diffusion rates can be influenced by mesospheric dust and ice formations which manifest themselves as PMSE in the polar regions. Temperatures were thus also evaluated using both strong and weak meteor echoes at the peak height. Meteor temperature estimates made at the peak height using only strong echoes, with the exception of the 33.2 MHz temperatures at Davis Station, show there is quite good agreement between the AURA based meteor temperatures and both OH and satellite temperatures during the course of the year to within ± 5 K. This range increases during the southern hemisphere summer months to approximately ± 10 K. This difference could possibly be attributed to variation in peak height of the meteor distribution with the peak height moving away from the mean height of the OH emission layer. All three locations however show that weak echoes that correspond to low SNR and electron trail densities serve to produce cooler temperatures and thus bias meteor temperature estimates. Unlike the 33.2 MHz results from Davis, the Darwin 33.2 MHz meteor temperatures do not exhibit the same offset observed. In fact the difference between the 55 MHz and other temperature estimates appears to be slightly less at BP compared with those made at Davis Station. This result could possibly suggest a latitudinal dependence on meteor diffusion coefficient estimates which would subsequently influence meteor temperature estimates. This effect is more prevalent with observations made at 33.2 MHz

compared with 55 MHz.

Chapter 9

Summary

This thesis has covered the development, refinement and modifications to a high-powered hybrid Very High Frequency (VHF) Sratospheric Tropospheric (ST)/meteor radar with the focus on development of the meteor radar. This summary will draw together the main aspects of the development of the meteor radar, results from statistical comparisons of observed atmospheric parameters from multiple independent co-located instruments and suggestions on further work.

In Chapter 2, an overview of meteor radar was presented along with derivations of some key results that are used in basic meteor radar observations including meteor diffusion coefficient and background wind velocity estimates. The derivation of meteor angle-of-arrival (AOA) was reproduced from the work of Jones et al. [1998] which also highlighted a key source of error on AOA estimates which arises from phase errors introduced from mutual coupling between antennas. This was touched upon later in Chapter 3 as the motivating factor for the use of an interferometer for the reception of meteor echoes. The basic operational principles behind MF radar, satellite and airglow observations were covered with references to more detailed descriptions provided.

In Chapter 3, radar hardware was discussed with particular attention paid to the development of the high-powered meteor radar system at BP. Descriptions of the physical hardware and functionality of the meteor radar systems used within this study along with operational parameters were presented. A fundamental overview of the radar acquisition process was presented as an understanding of this process is required in order to understand the processes outlined in Chapter 6 for determining characteristics such as echo

power and line charge density of meteor echoes. This discussion of the acquisition process equally applies to MF radar. As a part of the description of the high-powered meteor radar hardware, two key elements of the system were also introduced; the high-powered transmit antenna and the high-powered 1:2 splitter-combiner. The design, modification, testing and implementation of these two key aspects of the radar hardware are discussed in detail in Chapters 4 and 5. The development of this system played an important role in verifying the echo rate formula first published by McKinley [1961], but also helped to boost meteor echo rates with the aim of improving the statistical reliability of the meteor data. The MF radar systems of Buckland Park (BP) and Davis Station are also described in more detail in terms of the hardware configuration and operational modes.

In Chapter 4, the design details, numerical modeling, prototype test results and fabrication of the required high powered transmit antenna were covered. The design simulated with *EZNEC* proved to be successful, however in the final construction of the antenna, the antenna elements were not quite the right length, which resulted in the antenna feed point impedance having some reactance and thus not equaling $200 \pm 0.1j\Omega$ as simulated. In order to account for this a small tuned circuit consisting of a stub capacitor and inductor was designed by Broadband Propagation. Details for the key steps in fabrication and assembly of the antenna were presented for future reference. The antenna underwent two stages of evolution to investigate the performance of the design. The first generation involved using only one VTX PA module to ensure the transmission performance of the antenna met the design specification and also formed a stop-gap solution while the development of the 1:2 splitter-combiner took place. Once the 1:2 splitter-combiner was constructed, the antenna was then upgraded to its full power handling capability of 80 kW peak power; i.e. 40 kW per arm. Despite a single incident where a connector was not correctly tightened, the antenna performed flawlessly and continues to do so. Given the solid performance of the antenna, Broadband Propagation and ATRAD have adopted the design which is now used in meteor systems on King George Island in the Antarctic circle as well as Kunming and Wuhan in China.

Chapter 3 discussed in detail the second key piece of the BP high-powered meteor radar system in the the form of a splitter-combiner. This was used to provide two feeds to the meteor Tx antenna prior to upgrading to the STX-II transmitter. As discussed in Chapter 3, initially a quadrature split-

ter was designed and prototyped as this would have provided an in-phase and quadrature-phase output to the antenna. The design proved too temperamental and as such a more robust Wilkinson design with Gysel modification was designed and implemented. Chapter 5 details the design process of the 1:2 splitter combiner as well as highlights the modifications made and implemented in the design of the second generation splitter-combiner that improved the overall performance of the splitter-combiner design. The second generation combiner also included digital logic for sampling the forward and reflected power from the sum-port for remote monitoring of power levels. The second generation splitter-combiner is currently in use with new STX-II transmitter at BP and serves to combine the two standard outputs from the STX-II transmitter into a single output which is then split into six separate channels for stratospheric tropospheric observations.

In Chapter 6, the verification of the echo rate formula published in McKinley [1961] was achieved through operating the BP meteor radar at varying transmit power levels in order to establish experimental echo rate curves as a function of power. The formula in McKinley [1961] refers to the hourly count rate, and in order to determine a relation for the daily count rate for a given typical echo power, a constant of proportionality (β) was determined. In order for this to occur, a series of calibration experiments were required to determine what the output power from the radar was at each varying power level as well the receiver gain factor. It is important to note that all receivers were assumed to be balanced at time of manufacture and as such due to time constraints the results for a single receiver were taken to be indicative of all the other receivers. The procedures for performing the receiver gain and power curve calibration measurements are outlined in Chapter 6 and Appendix B respectively. The experiment was run on the BP meteor radar using two different transmitters and at similar times of the year in two different years with the results for β being equal in both cases. Both the VTX and the STX-II transmitter achieve similar average power, however they both have different peak power. The results from the experiment showed that the power terms in (6.1) are in fact the average power and not peak power, something which is not explicitly stated in McKinley [1961]. It is important to note that the value for β obtained essentially only represents a single point in the year and as such further observations are required as well as incorporating the existing work on the meteor response function (e.g. Cervera et al. [2004], Cervera and Elford [2004]).

Chapter 7 involved the statistical comparison of mesospheric wind measurements at Davis Station, Antarctica, and BP using the technique outlined in Section 7.1.1 and by Hocking et al. [2001]. Davis Station provided for three independent data sets, two of which utilised the same technique, that allowed for direct statistical comparisons to be made between MF radar and meteor radar wind observations. The statistical comparison technique provides two equations for relating the errors associated between two sets of measurements of the same quantity, however there are three degrees of freedom (σ_x, σ_y and g_0) in the two equations and in general this prevents an analytical solution from being found. Davis has two meteor radars which allowed for the reduction of the number of degrees of freedom; i.e. σ_x=σ_y. This result meant that the errors in the comparison of the two sets of meteor wind observations could be found and then applied to the comparisons of the meteor with the MF winds. Comparisons between meteor winds and both O-mode and X-mode MF observations were made with O-mode showing much better agreement with the meteor winds over a larger height range. This result is in strong agreement with previous observations; e.g. Tsutsumi and Aso [2005]. Differences in the quality of wind observations were observed between zonal and meridional directions and it is believed this can be partially attributed to the use of linear receive antennas for the meteor observations.

While it is generally accepted that the MF FCA technique underestimates the wind velocity [Holdsworth and Reid, 2004a,b, Tsutsumi and Aso, 2005], the comparisons of meteor winds with MF FCA and IDI winds show that there are in fact instances where the meteor winds underestimate the MF winds. Observation of a superposed epoch (24 hour period) of data appears to suggest that the underestimation of one technique compared with another occurs during the times where there are minimal scatterers available for the technique that appears to underestimate the wind. This result is not conclusive due to the limited number of meteor observations, however there is a strong indication in the data available that this could be the case. The overall finding was that there is typically a bias between meteor and MF winds of between 10 to 20% depending upon the MF technique used and the height at which winds are compared.

In Chapter 8, temperature estimates in the mesospheric region were determined using meteor diffusion coefficient data and an atmospheric pressure model. For reasons provided by Holdsworth et al. [2006], comparisons of meteor, airglow, satellite and falling sphere temperatures were performed at

the the peak height of the meteor distribution. Initially comparisons were made at a mean peak height, however it was later shown that at Davis, the peak height varies by as much as half a scale height, which has a significant impact upon the comparisons made. Temperatures were later estimated at the actual peak height of the meteor distribution and compared with airglow, satellite and falling sphere temperature measurements at Davis. Two independent pressure models were used to generate temperature estimates and it was shown that the pressure model does influence both the amplitude and mean value of the temperatures, however the pressure model does not account for everything observed in the temperature estimates. Following from the work of Younger et al. [2008], meteor diffusion coefficients were segregated into the strongest and weakest 25% echoes using the Signal-to-Noise Ratio (SNR) as the measure of echo strength. It was assumed that a direct linear relation exists between SNR measured for a particular echo and its corresponding line charge density. The results clearly indicated that weaker echoes lead to cooler temperature estimates. Temperature comparisons at BP were made between the meteor, airglow and satellite observations, while at Darwin comparisons were made between meteor and satellite observations.

The meteor temperature estimates show quite good agreement during the course of the year, however the meteor temperatures were generally much warmer than all other sources of temperature measurements included in this thesis during the course of the southern hemisphere summer months. During the course of the year, the meteor temperatures were in much closer agreement with both satellite and airglow temperatures. Another interesting feature is the $\sim$30 K temperature offset that is observed with the 33.2 MHz meteor temperatures which is not present in the Darwin results. There is a slight offset present between the 55 MHz temperatures and other airglow and satellite temperatures for Davis Station when comparing the Davis and BP comparisons, however this offset is not as prevalent as in the 33.2 MHz meteor temperature estimates. A statistical comparison between the 33.2 MHz and 55 MHz meteor temperature estimates from Davis was performed and despite the noticeable offset, significantly high correlations were found between the two data sets over the height range of the meteor distribution. The question of why there is such an offset with the 33.2 MHz temperatures at Davis Station is still yet to be answered. Dyrud et al. [2001] and Hall [2002] have shown that anomalous diffusion of meteor trails takes place at heights greater than 94 km. The maximum peak height at which meteor

temperatures were estimated for the 33.2 MHz system was 92 km, so it is quite likely the reason for the observed offset in meteor temperatures will be found elsewhere. Comparisons of temperatures with SABER temperatures at BP and Darwin showed good agreement between the mean values, however the SABER temperatures lacked the same annual variation characteristics present in the other temperature estimates. This is thought to be due to the use of an early revision of the SABER data provided and not indicative of the performance of the SABER instrument itself.

This thesis has detailed the development and refinement of a hybrid high-powered ST/meteor radar system along with comparisons of wind and temperature estimates made between meteor radar, MF radar, satellite, airglow and falling sphere observations. The results produced from meteor observations are certainly comparable to other accepted techniques used to measure mesospheric winds and temperatures, however further refinement of the techniques is required; particularly in regards to temperature estimates. Further investigations into the discrepancies between results of the meteor technique and other techniques included within this thesis will serve to better our understanding of the MLT region. While this thesis has served to answer questions about the reliability of the meteor technique for use in MLT studies, some questions were not completely resolved due to a lack of data which would have made some results more conclusive. It has also served to identified new questions to be answered in future work. Some of the key questions raised are:

- Does the increased number of echoes from using the high-powered meteor radar result in an increase in the number of low line charge density echoes that would bias meteor temperatures if included in the temperature analysis?
- What exactly is the relationship between the measured SNR and electron line charge density?
- Is there some form of latitudinal dependence which needs to be accounted for when determining meteor diffusion coefficients at different frequencies?

Along with answering these questions, better understanding of the meteor technique and its statistical reliability can be achieved through further

experimentation and analysis of data. Due to time constraints, answers to the questions identified within this study could not be found, but in time and with further experimentation the answers to these questions will be found!